

ORIGINAL ARTICLE

Pancreatic cancer heterogeneity and response to Mek inhibition

K Pedersen^{1,9}, F Bilal^{1,2,3,9}, C Bernadó Morales^{1,2}, MT Salcedo^{4,5}, T Macarulla^{4,5}, D Massó-Vallés^{1,3}, V Mohan⁶, A Vivancos⁷, M-J Carreras⁴, X Serres⁴, M Abu-Suboh⁴, J Balsells⁴, E Allende⁴, I Sagi⁶, L Soucek^{1,3,8}, J Tabernero^{1,2,4,5,7} and J Arribas^{1,2,3,8}

Our increasing knowledge of the mechanisms behind the progression of pancreatic cancer (PC) has not yet translated into effective treatments. Many promising drugs have failed in the clinic, highlighting the need for better preclinical models to assess drug efficacy and characterize mechanisms of resistance. Using different experimental models, including patient-derived xenografts (PDXs), we gauged the efficacy of therapies aimed at two hallmark lesions of PCs: activation of signaling pathways by oncogenic KRAS and inactivation of tumor-suppressor genes. Although the drug targeting inactivation of tumor suppressors by DNA methylation had little effect, the inhibition of Mek, a K-Ras effector, in combination with the standard of care (chemotherapy consisting of gemcitabine/Nab-paclitaxel), reduced the growth of three out of five PC-PDXs and impaired metastasis. The two least responding PC-PDXs were composed of genetically diverse cells, which displayed sensitivities to the Mek inhibitor differing by > 10-fold. Unexpectedly, our analysis of this genetic diversity unveiled different KRAS mutations. As mutation in KRAS occurs early during progression, this heterogeneity may reflect the simultaneous appearance of different malignant cellular clones or, alternatively, that cells containing two mutations of KRAS are selected during tumor evolution. *In vitro* and *in vivo* analyses indicated that the intratumoral heterogeneity, along with the selective pressure imposed by the Mek inhibitor, resulted in rapid selection of resistant cells. Together with the gemcitabine/Nab-paclitaxel backbone, Mek inhibition could be effective in treatment of PC. However, resistance because of intratumoral heterogeneity is likely to develop frequently, pointing to the necessity of identifying the factors and mechanisms of resistance to further develop this therapy.

Oncogene (2017) 36, 5639–5647; doi:10.1038/onc.2017.174; published online 5 June 2017

INTRODUCTION

Since cancer statistics have been available, the overall 5-year survival rate of pancreatic cancer (PC) patients has remained despairingly low (< 5%) (recently reviewed in Ryan *et al.*¹). In 1997, treatment with the DNA-damaging drug gemcitabine (Gem) was shown to result in clinical benefit and slightly improved survival.² Since this modest advance, many combinations of Gem with other drugs have been tested. However, it was only recently shown that the combination of Gem with Nab-paclitaxel (Nab-P), a drug that stabilizes microtubules, slightly improves the results of Gem alone.³ Foreseeably, unless an unexpected development takes place, in the near future therapies against PC will include the Gem/Nab-P chemotherapy backbone.

This lack of effective treatments contrasts with our expanding knowledge of the mechanisms that lead to progression of pancreatic ductal adenocarcinomas (PDACs), which represent > 85% of all types of PC. In the vast majority of cases, the proto-oncogene KRAS is activated by point mutations and two tumor-suppressor genes, CDKN2A and TP53, are inactivated.⁴ Activated K-Ras is not only required for PDAC initiation, but also for progression and metastatic growth.⁵ Along the same lines, reactivation of tumor-suppressor genes is predicted to inhibit PDAC development (see, for example, Xue *et al.*⁶).

With this information in hand, several compounds to inhibit PDAC progression have been developed. As repeated attempts to pharmacologically inhibit activated K-Ras have failed, efforts have shifted toward targeting its downstream effectors, particularly the mitogen-activated protein kinase kinase (Mek)–extracellular signal-regulated kinase (Erk) pathway, whose continuous activation seems to be required for the progression of PDAC.⁷ On the other hand, inactivation of p16 (encoded by CDKN2A) occurs frequently by epigenetic silencing through DNA methylation.⁸ Thus, azacitidine (Aza; commercial name, Vidaza), an inhibitor of DNA methyltransferases, has been proposed to inhibit cell proliferation by inducing re-expression of p16 and other epigenetically silenced tumor-suppressor genes.⁹

In this work, we analyzed the effect of drugs targeting Mek and DNA methylation, in combination with chemotherapy, on PC growth. As a model, we used PC cell lines, as well as PC patient-derived xenografts (PC-PDX), which retain many of the characteristics and heterogeneity of the original tumors. Although targeting DNA methylation had limited effects, Mek inhibition effectively reduced the growth of three out of five PC-PDXs. Interestingly, the least responding PDXs were heterogeneous and, within their cellular components, we found cells with primary resistance to the Mek inhibitor. Therefore, it is likely that inter and intratumor

¹Preclinical Research Program, Vall d'Hebron Institute of Oncology (VHIO), Barcelona, Spain; ²CIBER-ONC, Barcelona, Spain; ³Department of Biochemistry and Molecular Biology, Universitat Autònoma de Barcelona, Campus de la UAB, Bellaterra, Spain; ⁴Vall d'Hebron University Hospital (HUVH), Barcelona, Spain; ⁵Universitat Autònoma de Barcelona, Barcelona, Spain; ⁶Department of Biological Regulation, Weizmann Institute of Science, Rehovot, Israel; ⁷Clinical Research Program, Vall d'Hebron Institute of Oncology (VHIO), Barcelona, Spain and ⁸Institució Catalana de Recerca i Estudis Avançats (ICREA), Barcelona, Spain. Correspondence: Dr J Arribas, Vall d'Hebron Institute of Oncology (VHIO), C/Natzaret, 115-117, Barcelona 08035, Spain.

E-mail: jarribas@vhio.net

⁹These authors contributed equally to this work.

Received 21 February 2016; revised 29 March 2017; accepted 19 April 2017; published online 5 June 2017

heterogeneity will limit the efficacy of this therapy. Future elucidation of the mechanism(s) of resistance is warranted to allow the development of complementary therapies and/or to help define markers that identify the patients, which are most likely to benefit from Mek inhibition.

RESULTS

Effect of different drugs on the proliferation of PC cell lines

To identify effective and clinically relevant combinations for the treatment of PC, we chose the chemotherapeutic agents Gem, Aza and Nab-P. In addition, we selected MEK162, a drug that targets a signal transducer putatively required by PDACs to progress, namely the Mek kinase.

Dose-response experiments showed that the three chemotherapeutic agents inhibited the growth of the pancreatic cell line MIA PaCa-2 (Figure 1a, left). The same drugs had similar effectiveness, that is, comparable IC50s against three additional PC cell lines (Panc 10.05, HPAF-II and CFPAC-1) (Figure 1b). In contrast, IC50s of the Mek inhibitor varied from ~37.5 nM in MIA PaCa-2 cells to ~800 nM in CFPAC-1 cells (Figure 1a, right and b).

Gem, Nab-P and MEK162 increased apoptosis, as determined by the percentage of cells in the sub-G1 phase, whereas Aza induced a marked arrest in the G2/M phase (Figure 1c).

To test drug combinations, first we analyzed the effect of Gem, Nab-P and Aza at concentrations corresponding to ~IC25. The combination Gem/Nab-P inhibited cell proliferation more

efficiently than the combination Aza/Nab-P, although both were effective (Figure 1d). The triple combination was even more effective; unfortunately, it was excessively toxic *in vivo* (Supplementary Figure S1). Thus, we focused on the Gem/Nab-P combination as a backbone to add additional drugs. In this context, MEK162 increased the efficacy of Gem/Nab-P (Figure 1e).

Based on these results, we proceeded to determine the efficacy of selected drug combinations *in vivo*.

Effect of drug combinations *in vivo*

Compared with xenografts from established cell lines, PDXs better recapitulate the architecture as well as the molecular and cellular heterogeneity of the tumors from which they are derived.¹⁰ We therefore established a collection of PC-PDXs (Supplementary Figure S2A) in NOD-SCID mice. The clinical follow-up of the patients that donated samples showed that tumors, which successfully engrafted in immunodeficient mice tended to be more aggressive (Supplementary Figure S2B). For the subsequent studies, we used PDXs from four primary tumors and one liver metastasis (Supplementary Figure S2C); all of them retained the histopathological and genetic characteristics of the original tumors and conserved them during the successive passages (Supplementary Figure S3 and data not shown).

In the treatment experiments, we switched to BALB-c Nude mice because Gem was severely toxic to NOD-SCID mice (data not shown). Comparison of effectiveness of the two chemotherapy regimens demonstrated, in agreement with the results shown in

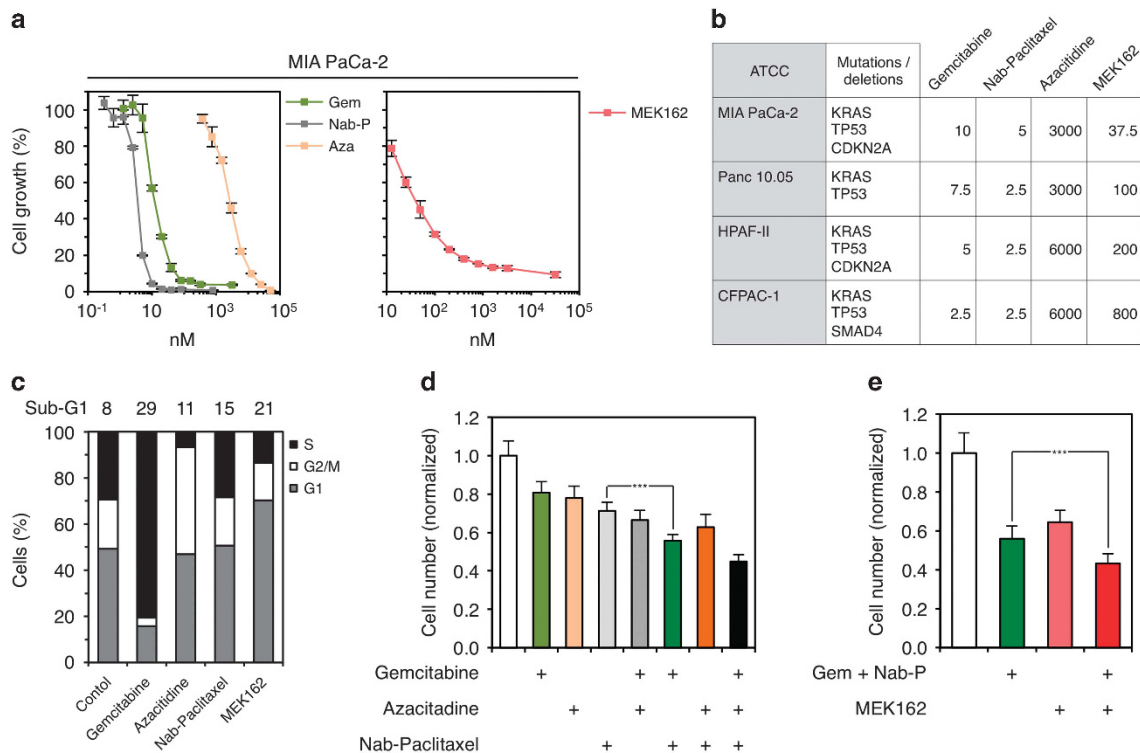


Figure 1. Effects of different drugs and drug combinations on the proliferation of PC cell lines. **(a)** MIA PaCa-2 cells were treated with different concentrations of the indicated drugs during 3 days. Then, cell numbers were estimated with the crystal violet staining assay. The results are expressed as averages and the error bars correspond to 95% confidence intervals of three independent experiments. *P*-values were calculated using the two-sided Student's *t*-test. **(b)** The indicated cell lines, which bear mutations or deletions in the genes shown, were analyzed as in **a**. IC50 values are shown. **(c)** MIA PaCa-2 cells were treated as in **a** with drug concentrations corresponding to IC50s for 24 h. Then, the percentages of cells in each phase of the cell cycle were analyzed by propidium iodide and flow cytometry. The percentages of cells in the sub-G1 area and excluded from the cell cycle analysis are positioned at the top. **(d, e)** MIA PaCa-2 cells were treated with drug concentrations corresponding to IC25s for 3 days. Then, cell numbers were estimated with the crystal violet staining assay. The results are expressed as averages and the error bars correspond to 95% confidence intervals of three independent experiments. *P*-values were calculated using the two-sided Student's *t*-test.

Figure 1, that both Gem/Nab-P and Aza/Nab-P impaired the growth of the PDXs, although the combination Gem/Nab-P was slightly more effective (Figure 2a). At the end of the experiment, tumors were removed and weighted; the weights of the tumors confirmed the results obtained by measuring tumor volumes (Figure 2b).

It should be noted that we used the highest concentrations of drugs that did not have overt toxic effects when administered in cycles corresponding to those used in patients (Supplementary Figure S1). The effects on tumor growth of the combination 40 mg/kg Gem/20 mg/kg Nab-P was similar to that of 20 mg/kg Gem/10 mg/kg Nab-P; however, the former had a toxic effect that induced weight losses > 10% (Supplementary Figure S5).

Next, we tested if the addition of MEK162 added efficacy to the Gem/Nab-P combination. The Mek inhibitor improved the effect of

chemotherapy in three out of five PDXs in a statistically significant manner (Figures 3a and b). In one of the PDXs (PC-PDX10), the effect on tumor volume was not significant, but we observed a statistically significant reduction in tumor weight of 39.2% (Figure 3b).

To monitor the effect of MEK162 at the molecular level, we determined the levels of phospho-Erk1,2 in tumors at different time points in a new experiment. As expected, the activity of Mek was inhibited after administration of MEK162 (Figure 4, days 12 and 17, see Supplementary Figure S6 for the specificity of the phospho-Erk1,2 staining) but quickly recovered after two days (Figure 4, day 14). To quantify the necrotic and fibrotic areas, we stained sections from resected tumors with Picrosirius red. Interestingly, the percentages of necrotic and fibrotic areas were higher in all the tumors treated with MEK162 (Figure 4, day 31 and

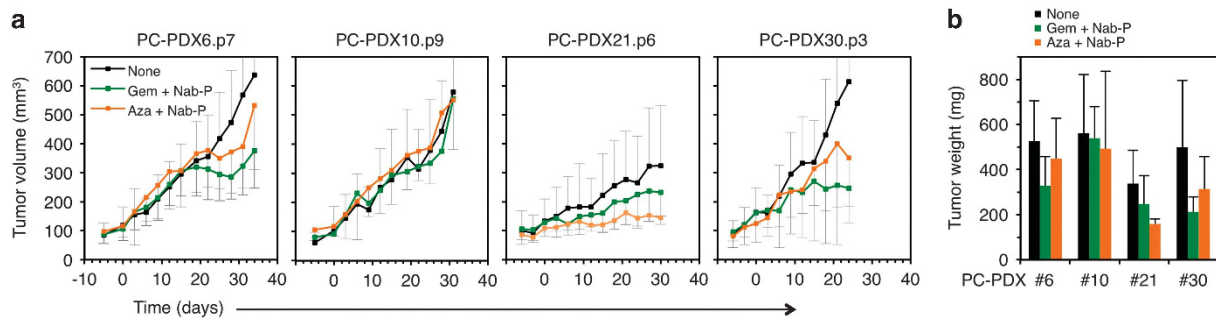


Figure 2. Effect of Nab-P plus Gem or Aza on the growth of PC-PDXs. **(a)** The volumes of PDXs established from three infiltrating ductal adenocarcinomas (PC-PDX6, 10 and 21) and one liver metastasis (PC-PDX30), treated as indicated (see also Supplementary Figure S1A), were determined at different time points ($n=6$ in each group). The passage (p) used is indicated by the corresponding number. Error bars correspond to 95% confidence intervals. **(b)** At the end of the experiments, mice were killed and the tumors removed and weighed. The results are expressed as averages and the error bars correspond to 95% confidence intervals.

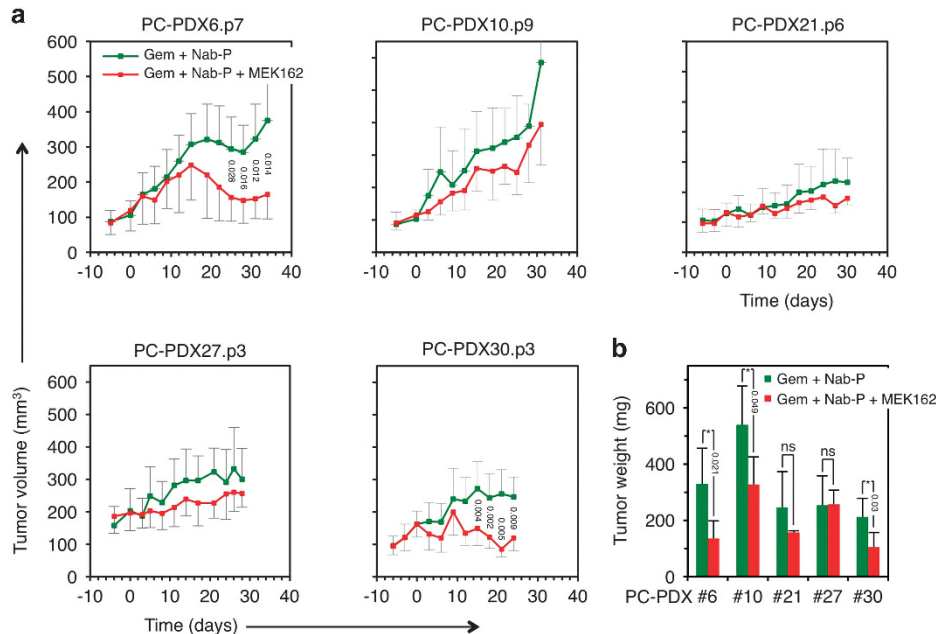


Figure 3. Effect of Mek inhibition on the growth of PC-PDXs treated with backbone chemotherapy. **(a)** The volumes of PDXs established from four infiltrating ductal adenocarcinomas (PC-PDX6, 10, 21 and 27) and one liver metastasis (PC-PDX30), treated as indicated (see also Figure 4a), were determined at different time points ($n=6$ in each group). Error bars correspond to 95% confidence intervals. P -values were calculated using the two-sided Student's t -test. **(b)** At the end of the experiments, mice were killed and the tumors removed and weighed. The results are expressed as averages and the error bars correspond to 95% confidence intervals. P -values were calculated using the two-sided Student's t -test.

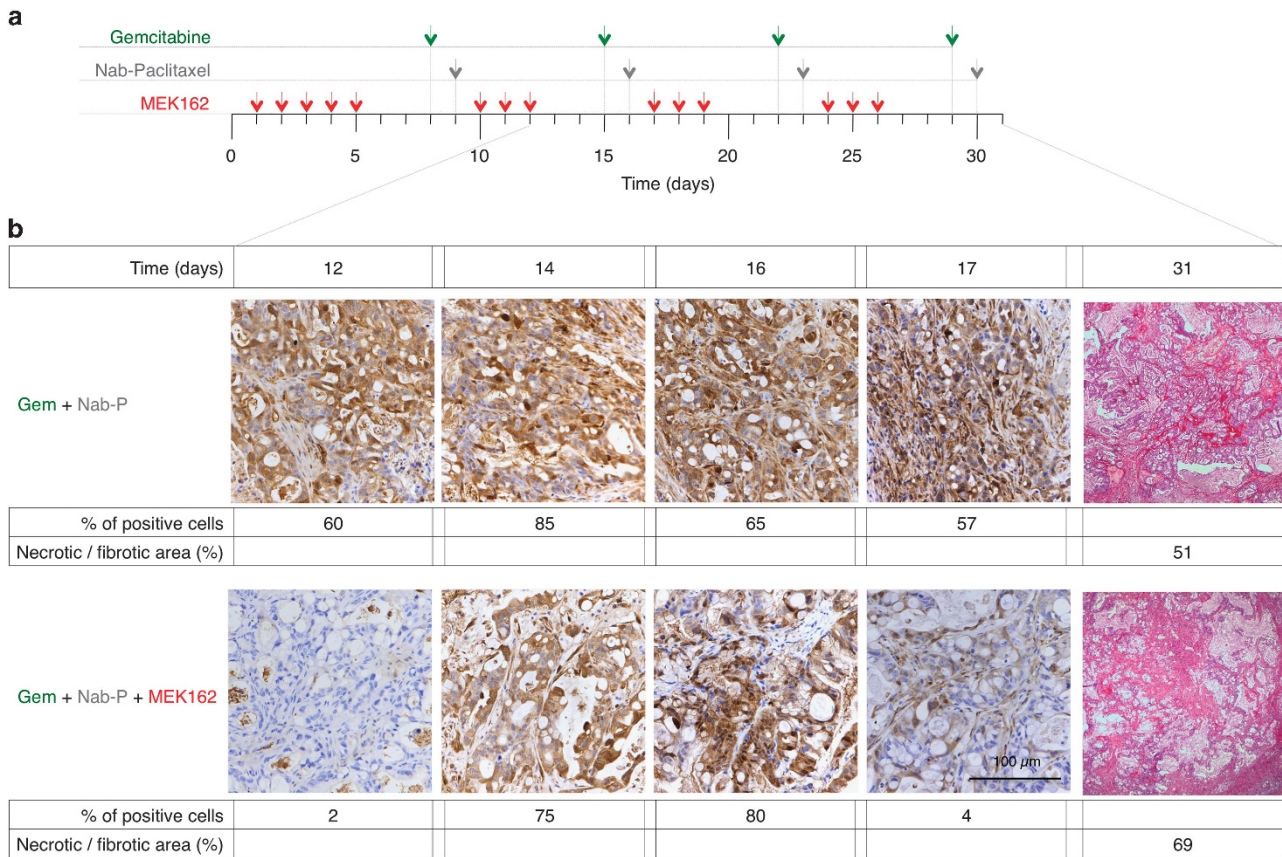


Figure 4. Effect of MEK inhibition on phospho-Erk1,2 levels or tumor necrosis/fibrosis in tumors treated with backbone chemotherapy. **(a)** Schematic drawing showing the drug administration regimes. **(b)** At the indicated time points, mice bearing PC-PDX6.p8 treated as in Figure 3 were killed and samples from the tumors were stained with anti-phospho-Erk1,2 or, to visualize the necrotic/fibrotic areas, with picosirius red. The number of cells positive for phospho-Erk1,2 or the percentage of necrotic/fibrotic areas were quantified (see also Supplementary Table S1).

Supplementary Table S1), indicating that the effect of the Mek inhibitor on tumor growth was likely underestimated in the analysis of tumor volume or weight.

In summary, MEK162 adds antitumor efficacy to the chemotherapy backbone used as the standard of care in three out of five PC-PDX models tested.

Effect of the Gem/Nab-P/MEK162 combination on the growth of orthotopic xenografts

Although the desmoplastic component of the original tumor was preserved in the PDXs implanted subcutaneously (Supplementary Figures S3A and B), orthotopic models may better recapitulate the desmoplasia of PDACs.¹¹ Thus, we treated mice orthotopically implanted with PC-PDX10. Also in this setting, MEK162 inhibited tumor growth (Supplementary Figure S7A). In agreement with the higher percentage of fibrotic area observed in subcutaneous tumors (Figure 4b, 31 days and Supplementary Table S1), orthotopic tumors treated with MEK162 showed an increased content in extracellular collagen deposition and a higher level of alpha-smooth muscle actin positive cells (Supplementary Figure S7B).

In order to precisely quantify the effect of MEK162 in the orthotopic setting, we injected MIA PaCa-2 cells expressing luciferase (MIA PaCa-2/Fluc) in the pancreases of BALB-c Nude mice. In this orthotopic model, the backbone chemotherapy did not affect tumor growth (Supplementary Figure S8A). This result

highlights the differences between PC-PDXs and established cell lines, whereas the first model is sensitive to the maximal tolerated dose of Gem/Nab-P (Supplementary Figure S5A). Given the efficacy in the clinical setting of Gem/Nab-P,³ these results further support the relevance of the PDX models.

However, for consistency with the rest of our *in vivo* analyses, we maintained Gem/Nab-P in the treatments when analyzing the effect of MEK162 in the orthotopic models of MIA PaCa-2 cells. As a control, MIA PaCa-2 cells also were injected subcutaneously in another group of mice. In both models, the Mek inhibitor added efficacy to Gem/Nab-P approximately to the same extent (Figures 5a-c).

Next, we determined the effect of these drug combinations on the metastatic growth of MIA PaCa-2/Fluc cells. From the pancreas, these cells metastasize primarily to liver, spleen and lung. Treatment with Gem/Nab-P alone did not significantly reduce the metastatic growth because three out of four mice exhibited metastases in both treated and control groups (Supplementary Figure S8B). In an independent experiment, analysis of *ex vivo* luminescence showed metastases in 8 out of 10 mice treated with the Gem/Nab-P backbone (Figure 5d and Supplementary Figure S8C). The secondary tumors were detected in lung, spleen, liver and diaphragm. Remarkably, addition of MEK162 reduced the metastatic growth; we detected only one spleen metastasis in 10 mice treated with the triple combination (Figure 5d and Supplementary Figure S8C).

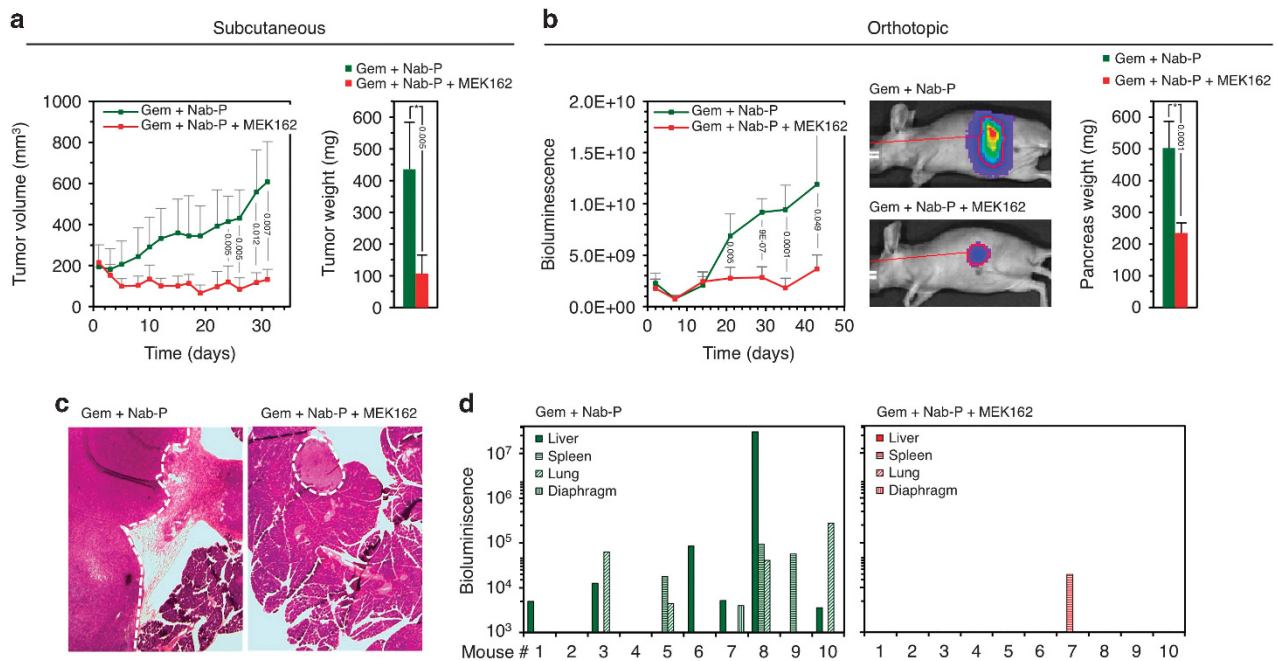


Figure 5. Effect of MEK inhibition on the progression of subcutaneous and orthotopic xenografts treated with backbone chemotherapy. **(a, b)** MIA PaCa-2 cells expressing luciferase were injected subcutaneously **(a)** or orthotopically **(b)**. Tumor growths were monitored by assessing volumes **(a, left)** or luminescence **(b, left)**. Representative luminescence images are shown **(b, middle)**. At the end of the experiments, mice were killed and the subcutaneous tumors or pancreases were removed and weighed **(a and b, right bar graphs)**. The results are expressed as averages and the error bars correspond to 95% confidence intervals. *P*-values were calculated using the two-sided Student's *t*-test. **(c)** Pancreases were removed at the end of the experiment shown in **b**. Samples from these tumors were stained with hematoxylin-eosin. Representative images are shown and tumor areas are marked with white dotted lines. **(d)** At end of the experiment described in **b**, metastatic growths were assessed by *ex vivo* quantification of luminescence in liver, spleen, lung and diaphragm (see also Supplementary Figure S8C).

These results further show the effectiveness of the Gem/Nab-P/MEK162 combination to impair growth of pancreatic carcinomas and their metastatic progression.

Intratumoral heterogeneity and resistance to MEK162

Intratumoral heterogeneity has emerged as an underlying mechanism of tumor evolution and adaptation to anticancer therapies.¹² To characterize the potential impact of tumor heterogeneity on the resistance to MEK162, we analyzed the mutational profile of the different PC-PDXs by sequencing a panel of 57 cancer-related genes.

As expected, we found mutations in KRAS and TP53 in all cases (Figure 6a). Intriguingly, in two of the PC-PDXs, 10 and 21, we found different mutations in KRAS, indicating that these PC-PDXs may be composed of different clones. Specifically, in the PC-PDX21, in addition to the predominant mutation (c.G35T:p.G12V), we found two additional KRAS mutations (c.G35A:p.G12D and c.G34C:p.G12R), albeit with low allele frequencies (2% and 1%, respectively); in PC-PDX10, we found the c.G35T:p.G12V mutation in addition to the predominant one, c.G35A:p.G12D (Figure 6a). To confirm the existence of these mutations, we analyzed their presence by digital droplet PCR (ddPCR). All the mutations were found in samples from the original tumor and, importantly, despite their low frequency, all but one were also present in the PDXs, further reinforcing the reliability of this experimental model (Supplementary Figure S4).

To further analyze intratumoral heterogeneity in the two PDXs resistant to Mek inhibition, we established *in vitro* cultures from PC-PDXs 21 and 27 and isolated individual cell colonies. The panel of cancer-related genes was sequenced from the fastest growing colonies. Mutations in the SMAD4, STK11, CDKN2A and VHL genes showed that at least three of the four colonies from PC-PDX21 contained genetically distinguishable cells (Figure 6b), indicating

that PC-PDX21 is highly polyclonal. In addition, the low allele frequencies of some of the mutations identified indicated that even the isolated colonies contain more than one cell clone.

The sensitivities of the cells from the different colonies to the MEK inhibitor were different; their IC₅₀s ranged from ~30 nM to ~800 nM (Figure 6c) indicating that the original tumors were composed of cells with a wide range of tolerances to Mek inhibition. Although cells from the B2, B6 (PDX21) and C1, C2 (PDX27) colonies showed different sensitivities to MEK162 (Figure 6c), we did not find any difference in the sequences of the genes included in the gene panel (Figure 6b). Therefore, to determine if they were genetically different, we sequenced exome libraries prepared from these colonies. This analysis showed that all the colonies analyzed contain genetically distinguishable cells (Figure 6d).

The detected polyclonality suggests that the moderate responses of the PC-PDXs 21 and 27 to MEK162 could be because of the selection of pre-existing cells resistant to Mek inhibition. To test this hypothesis, we mixed (1:1) cells from colonies B2 and B6 and cells from colonies C1 and C2, cultured them in the presence or absence of MEK162 and followed the evolution of gene copies bearing the mutation LRRRC E193Q or FLT3 P934L by ddPCR. We used these mutation as genetic markers to follow the fate of resistant cells because they are present only in PC-PDX21-B6 or PC-PDX27-C1 cells, which, compared with the rest of cells isolated from PC-PDX21 or PC-PDX-27, are resistant to MEK162 (Figures 6c and d). Indeed, treatment with MEK162 increased the frequency of the mutations LRRRC69 E193Q or FLT3 P934L, showing that the selective pressure exerted by the Mek inhibitor led to selection of Mek-resistant cells within a relatively short period of time (Figure 6e).

It should be noted that although their frequencies (47% and 37% for LRRRC69 E193Q and FLT3 P934L, respectively) indicated heterozygosity, the enrichment induced by MEK162, shows that

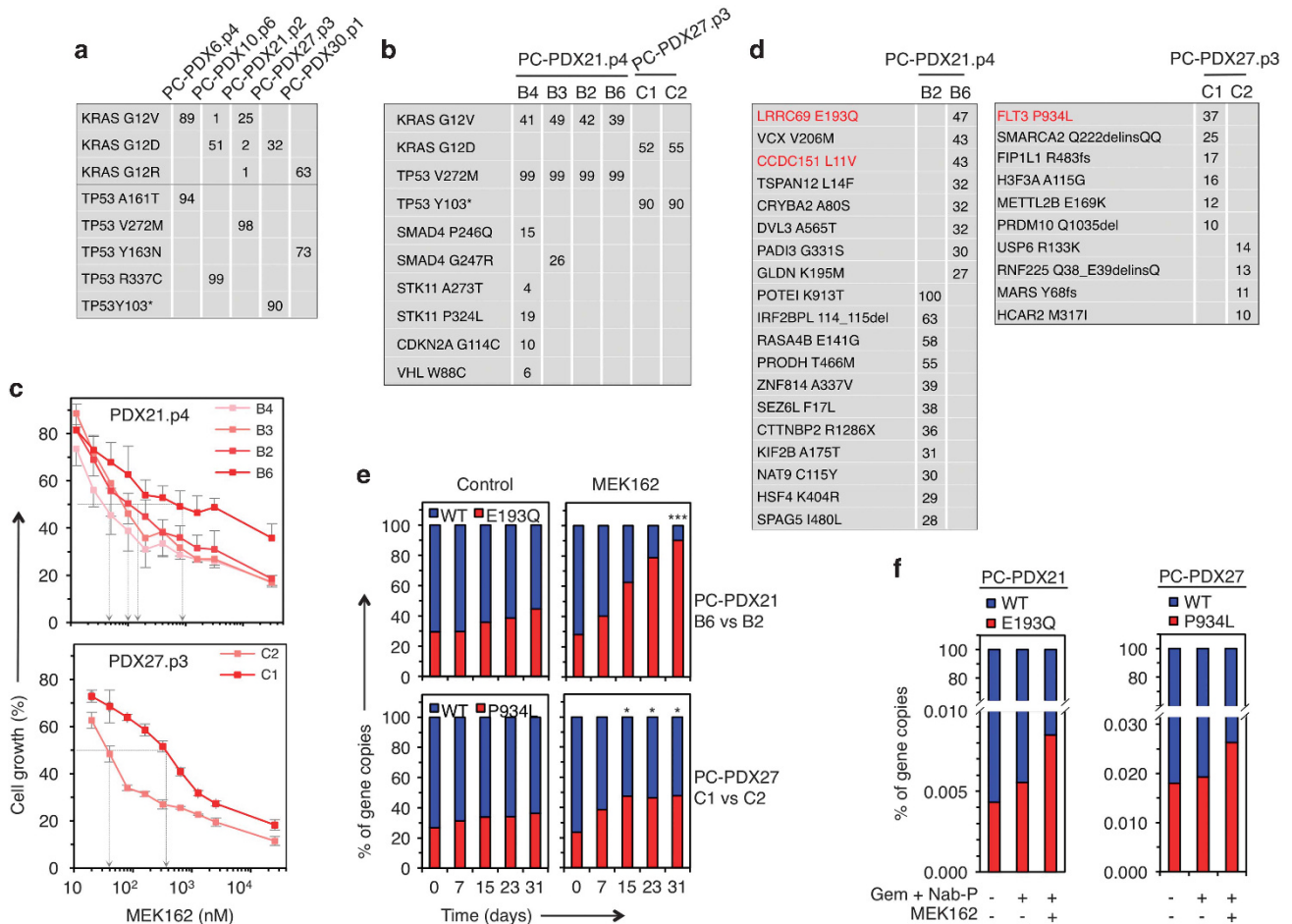


Figure 6. Intratumoral heterogeneity and response to MEK inhibition. **(a)** Sequences of a panel of 57 cancer-related genes were determined from the indicated PDXs. The allele frequencies of the mutations found are shown. **(b)** PC-PDX-21 and -27 were disaggregated and cultured *in vitro*. Several cell colonies (named B2, 3, 4, 6 and C1, 2) were isolated and sequences of the panels of 57 cancer-related genes were determined. The allele frequencies of the mutations identified are shown. **(c)** Cells from the different colonies were treated with different concentrations of MEK162. Then, cell number was estimated with the crystal violet staining assay. The results are expressed as averages and the error bars correspond to 95% confidence intervals of three independent experiments. **(d)** Exome libraries prepared from colonies B2, B6, C1 and C2 were sequenced. Mutations with allele frequencies higher than 10% in one of the colonies and non-detectable in the other are shown. **(e)** Cells from colonies B2 and B6 from PC-PDX21 (upper panels) or colonies C1 and C2 from PC-PDX27 (lower panels) were mixed 1:1 and cultured in the absence or presence of MEK162. At the indicated time points, the percentages of wild-type and mutant LRRRC69 E193Q or FLT3 P934L alleles were determined with ddPCR. The results are expressed as averages of three independent experiments. *P*-values were calculated using the two-sided Student's *t*-test. **(f)** The presence of LRRRC69 E193Q or FLT3 P934L mutant alleles were determined in DNA isolated from tumors resected after the indicated treatments of PC-PDX21 or PC-PDX27 (see Figure 3).

the LRRRC69 E193Q is homo- or hemizygous. After 1 month of treatment with the inhibitor, the frequencies of these mutations reached ~90% (Figure 6e, PC-PDX21) demonstrating that the resistant cells, homo- or hemizygous for LRRRC69 E193Q, overgrew the sensitive ones. Thus, the initial B6 colony most likely contained more than one cell clone. These results were confirmed by analyzing the dynamics of another mutation (CCDC151 L11V) (Supplementary Figure S8D).

In contrast with these results, treatment with MEK162 resulted in an allele frequency of ~50% for the mutation FLT3 P934L (Figure 6e, PC-PDX27), indicating that this mutation exists in heterozygosity.

To confirm *in vivo* the enrichment of resistant cells, we determined the frequencies of markers for resistant cells (mutations in LRRRC69 and FLT3 P934L) in PC-PDX21 and PC-PDX27 treated without or with MEK162. We found that these mutations were present at very low allele frequency (Figure 6f). However, xenografts after 1 month of treatment with MEK162 displayed an increase in the frequency of the mutant alleles

(Figure 6f and Supplementary Figure S8E), further supporting the conclusion that tumors likely become refractory to Mek inhibition through selection of primary resistant cells.

Collectively, these results show that Mek inhibition adds efficacy to chemotherapy. However, the selection of pre-existing cells resistant to the treatment may compromise the long-term efficacy of this therapy in a significant proportion of patients.

DISCUSSION

The lack of efficacy of the vast majority of anticancer therapies against PDACs highlights the need for predictive preclinical models that faithfully represent human tumors. Although genetically modified mice have proven formidably powerful for characterizing the factors and mechanisms involved in the progression of PDACs, their value in the development of novel therapeutic strategies has been limited. This has prompted the use of alternative models such as PDXs, which retain many of the

characteristics of the original tumors, including intratumor heterogeneity.¹³

Using this model, we have analyzed the efficacy of different therapies against PDACs. To be as close as possible to the clinical setting, we used therapeutic regimens that resemble those used in patients (Figure 4a and Supplementary Figure S1A). In addition, we assessed the potential of inhibition of Mek or inhibition of DNA methylation by asking if they add efficacy to the chemotherapeutic agents Gem and Nab-P, which will be included in the standard of care for PDAC patients in the near future.

The inhibitor of DNA methylation Aza had some promising antitumor effect in our models (Figures 1 and 2). Unfortunately, the combination Gem/Nab-P/Aza was toxic and could not be tested *in vivo*.

Importantly, our results clearly point to Mek inhibition as a potentially effective therapy in combination with the standard of care (Figures 3 and 5). However, it is noteworthy that IC50s for MEK162 vary 40-fold in different PC cell lines, all bearing an activating KRAS mutation (Figure 1b). Based on this result, one may expect that only some pancreatic tumors will be sensitive to MEK162. Our results support this possibility; two out of five PC-PDXs (21 and 27), despite having a KRAS mutation like the others, were insensitive to the Mek inhibitor, and one (PC-PDX10) had a reduction in tumor weight of only ~39% (Figure 3).

Initial evidence, mainly based on genetically modified mouse models, has shown the importance of desmoplasia, regulated by the hedgehog pathway, in the progression of PDAC.¹⁴ However, recent publications have cast doubts on these findings and instead proposed that the dense desmoplastic stroma encapsulates tumor cells restraining their growth and dissemination.^{15–17} In our PC-PDX model, Mek inhibition induced, concomitantly, higher levels of desmoplasia and reduced tumor progression (Figure 3 and Supplementary Figure S7), supporting the inhibitory effect of desmoplasia on PDAC progression. These results warrant future research on regulation of desmoplasia by Mek signaling.

Our results show for the first time that intratumor heterogeneity may represent a major drawback for this therapeutic strategy. From the two resistant PDXs, we isolated cells that responded very differently to Mek inhibition, with IC50 ranging from ~37.5 to 800 nM. Characterization of these cells clearly showed that they are genetically diverse and that they likely reflect the clonal evolution of the tumor. Furthermore, *in vitro* and *in vivo* analyses of individual cell colonies showed that the selective pressure imposed by Mek inhibition results in the rapid selection of resistant cells (Figure 6). This resistance may explain the lack of efficacy of Mek inhibition on advanced PC patients recently observed.¹⁸

As an interesting aside, the most widespread view assumes that acquisition of activating mutations in KRAS is one of the earliest steps in PDAC progression. Nevertheless, in two out of five PDXs we detected different KRAS mutations (Figure 6a and Supplementary Figure S4). The presence of different KRAS mutations in one single tumor may reflect the simultaneous appearance of different malignant cellular clones or, alternatively, that cells containing two mutations of KRAS are selected during tumor evolution.

In summary, our results indicate that Mek inhibition is relevant for the treatment of PC. Nevertheless, we anticipate that the selection of resistant cells will compromise the efficacy of this therapy. Thus, the elucidation of the mechanisms of resistance to Mek inhibitors will be the next step in refining this therapeutic strategy to improve long-term efficacy.

MATERIALS AND METHODS

Cell lines

The cell lines MIA PaCa-2, Panc 10.05, HPAF-II and CFPAC-1 were purchased from ATCC (Manassas, VA, USA). Unless otherwise stated, cells were grown

as described in Borroto *et al.*¹⁹ at 37 °C in presence of 5% CO₂ and in pancreatic medium: Dulbecco's modified Eagle's medium/F-12 (Invitrogen, Thermo Fisher Scientific, Waltham, MA, USA) supplemented with 8% fetal bovine serum, 2% horse serum, 2 mM L-glutamine and 1x antibiotic-antimycotic (Gibco, Thermo Fisher Scientific).

Cell proliferation

To determine proliferation, cells were seeded in at least two 96-well plates with 1000 cells in 80 µl per well, except for one column to which 80 µl of medium without cells was added to provide a background reference value. After 24 h, the cells were fixed in the first plate (time 0) by adding 80 µl 10% glutaraldehyde to each well followed by 30-min incubation. After washing wells with water, this plate was kept at 4 °C and later stained together with the other plates. In the rest of the plates, 80 µl of medium with or without various concentrations of drugs was added to all wells and then returned to the cell incubator for another 3 days. After fixation of cells, the wells were washed in water, dried for 5 min upside down on paper and then stained with a 0.1% crystal violet solution. Finally, the wells were washed, dried ON and assayed with 10% acetic acid and 560 nm absorbance measurements.

Cell cycle analysis

MIA PaCa-2 cells were analyzed for cell cycle progression after 24 h in the presence or absence of various combinations of drugs. First, cells were trypsinized, washed with 1X phosphate-buffered saline (PBS) and fixed with 70% ethanol for 30 min. After two washes in PBS, cells were incubated with DNA extraction solution (0.2 M Na₂PO₄, 0.1 M citric acid, pH=7.8) for 10 min at 37 °C. Finally, cells were incubated with propidium iodide/RNase solution (40 µg/ml PI/10 µg/ml RNase in 1X PBS) for half an hour followed by flow cytometric analysis.

Therapeutic compounds

Gem was purchased from a pharmacy as a 38 mg/ml perfusion solution. Nab-P and Aza were provided by Celgene (Summit, NJ, USA) as Abraxane (5 mg/ml) and Vidaza (25 mg/ml), respectively. Gem, Nab and Aza were diluted in 0.9% NaCl to 4 mg/ml, 2 mg/ml and 0.4 mg/ml before administration by intraperitoneal injection of 20, 10 and 2 mg/kg, respectively. The Mek inhibitor MEK162 was provided as powder by Novartis (Basel, Switzerland). Suspension of MEK162 in 10% Tween-80 was incubated ON at 4 °C before diluting 20-fold with 1% Na-carboxymethylcellulose and 0.5% methylcellulose, respectively. The final concentration of active MEK162 was 1.5 mg/ml and 6 mg/ml, which was administered by gavage to 15 mg/kg morning and evening.

PC-PDX mouse models

All animal studies were performed in accordance with ARRIVE guidelines and the three Rs rule of replacement, reduction and refinement principles. Mice were housed and treated according to protocols approved by the CEEA (Ethical Committee for the Use of Experimental Animals) at the Vall d'Hebron Institute of Oncology (VHIO), Barcelona, Spain. NOD-SCID and BALB-c Nude mice were purchased from Charles River Laboratory (Wilmington, MA, USA). Mouse weights were determined twice a week and recorded for every experiment.

The anonymized human samples used were part of the tissue biological material of the Vall d'Hebron University Hospital. The samples had been collected with a signed patient consent form and were used with the approval of the Ethics Committee of the Hospital. Heterotopic xenografts were generated from tumors of patients that underwent pancreatectomy at the hospital: when routine pathological gross examination of a resected pancreas led to the detection of a suspected neoplasia, a slice with a thickness of 1–3 mm was transferred to RPMI-1640 medium containing 1x antibiotic-antimycotic (Gibco, Thermo Fisher Scientific) and kept on ice; within approximately 30 min the tissue sample was cut into pieces of about 10 mm³ under sterile conditions, suspended in Matrigel (BD Biosciences, Franklin Lakes, NJ, USA) and transported to the specific pathogen free area of the animal facility. One tumor piece was implanted subcutaneously into the flank of two or three female 6-week-old NOD-SCID mice. When successfully grafted, tumors reached a size of around 750 mm³ they were transplanted to new mice. From the third round of transplantation, 6-week-old BALB-c Nude mice were used for further expansion of the xenografts.

The samples used for the generation of PC-PDX6, 10, 21 and 27 were classified as classic ductal adenocarcinomas during their pathological evaluation. The sample that produced PC-PDX30 originated from a needle biopsy of a liver metastasis in a patient with advanced PC. The passages of the PDX used in each experiment are labeled using the following nomenclature: PC-PDX6.p7 (PC-PDX6.Passage 7).

Animals from the same round of transplantation were randomized into the different experimental groups 2 days before the first treatment. Tumor size was evaluated every third day by caliper and tumor volume calculated using the formula: $\text{volume} = 0.5 \times \text{length} \times (\text{width}^2)$.

After the treatment ended, the animals were killed, tumors collected and fixed ON in neutral pH-buffered 4% formalin. A pathologist confirmed the histopathological characteristics of xenografts from the expansion phase and after the treatments. PDXs intended for two-photon microscopy analysis, were resected after perfusion with 0.9% NaCl followed by 4% formalin. The tissue samples were preserved by incubation in 30% sucrose in 1x PBS at 4 °C ON and subsequently embedded in OCT.

Hematoxylin–eosin, immunohistochemistry and fibrosis staining

Fixed tissue samples embedded in paraffin were sectioned at 5 μm thickness. For immunohistochemistry, sequential sections were deparaffinized, rehydrated and microwaved for 1 min in 0.01 M citrate buffer (pH 6.0) for antigen retrieval. Primary antibodies (against Ki67 (30-9; Ventana Medical System, Roche, Basel, Switzerland), CK19 (A53B/A2.26; Cell Marque, Sigma-Aldrich, St Louis, MO, USA), P53 (DO-7; Ventana Medical System, Roche), MUC1 (H23; Ventana Medical System, Roche), Ca19.9 (121SLE; Ventana Medical System, Roche) and P-ERK1/2 (Thr202/Tyr204; Cell Signaling, Danvers, MA, USA)) were applied for 2 h in blocking buffer (2.5% bovine serum albumin, 5% goat serum and 0.3% Triton X-100 in 1x PBS), followed by Vectastain ABC kit and DAB reagents (Vector Laboratories, Burlingame, CA, USA) visualization.

Picrosirius Red stain kit (Polysciences, Inc., Warrington, PA, USA) was used to stain for collagen types I and III according to the manufacturer instructions.

Images were obtained with an Olympus (Shinjuku, Tokyo, Japan) BX41 microscope and DP71 camera.

Two-photon microscopy and second harmonics generation

Unstained Xenograft tumors were cut 300 μm thick and visualized using a two-photon microscope (2PM:Zeiss LSM 510 META NLO; equipped with a broadband Mai Tai-HP-femtosecond single box tunable Ti-sapphire oscillator, with automated broadband wavelength tuning 700–1,020 nm from Spectraphysics, Newport (Irvine, CA, USA), for two-photon excitation) with Plan Achromat 20 \times /0.8 (Carl Zeiss, Oberkochen, Germany). For collagen second harmonic imaging, a wavelength of 880 nm was used.

Transduction

To express Fluc in MIA PaCa-2 cells, the corresponding gene was cloned in the lenti-viral vector pLEX (Open Biosystems, Thermo Fisher Scientific). Lenti viruses were prepared with HEK293T and Trans-Lenti Packaging kit from Open Biosystems (Thermo Fisher Scientific). Virus containing supernatants were filtered with 0.45 μm polyvinylidene difluoride filters (Merck Millipore, Billerica, MA, USA) and medium from 1 cm^2 packaging cells was used to infect 2 cm^2 recipient cells at approximately 35% confluence. Approximately 90% infection efficiency was verified 3 days after transduction in a parallel control using pLEX-GFP. Transduced cells were selected with 0.8 $\mu\text{g}/\text{ml}$ puromycin, starting 3 days after infection, and subsequently maintained with 0.4 $\mu\text{g}/\text{ml}$ puromycin in the growth media.

Orthotopic mouse model of PC

MIA PaCa-2/Fluc cells were suspended in 1 \times PBS and 50% Matrigel to 80 000/ μl . Using a 27 gauge needle, 10 μl cell suspension was injected into the tail of the pancreas of 7-week-old female BALB-c Nude mice. The rate of tumor growth was monitored weekly by *in vivo* bioluminescence imaging with the IVIS-200 imaging system from Xenogen (PerkinElmer, Waltham, MA, USA). The day after the last treatment, the mice were killed and all major organs resected in order to determine the existence of distant metastasis by IVIS imaging.

Orthotopic tumors of PC-PDX10 were prepared by injection of 10 μl cell suspension in NOD-SCID mice. The cell suspension was prepared from a subcutaneously grown PDX of ~500 mg that was minced with a scalpel, digested in 10 ml Dulbecco's modified Eagle's medium/F-12 containing

500 U/ml Collagenase type IV (Worthington, Lakewood, NJ, USA) at 37 °C for 30 min, washed in pancreatic medium and then 1x PBS, and finally suspended in 0.5 ml 1 \times PBS and 0.5 ml Matrigel.

Primary cell cultures

A subcutaneously implanted PC-PDX21 of app 750 mm^3 was resected, minced with a scalpel and seeded in a 10 cm standard culture dish with pancreatic medium. The medium was changed twice a week and after 3 weeks individual colonies of epithelial cells were collected with drops of 0.05% Trypsin-EDTA (Gibco, Thermo Fisher Scientific).

Amplicon-Seq VHIO-card panel

An initial multiplex-PCR with a proof-reading polymerase was performed on the samples, using a panel of over 600 primer pairs targeting frequent mutations in oncogenes plus several tumor suppressors, covering 57 different genes (Supplementary Table S2). SBS-Illumina compatible libraries were generated by adapter ligation after end repair and A-tailing of amplicon products.

Indexed libraries were pooled and loaded onto a MiSeq instrument and sequencing performed (2X100). Initial alignment was performed with BWA after primer sequence clipping and variant calling was done with the GATK Unified Genotyper (Cambridge, MA, USA) and VarScan2 (St Louis, MO, USA) followed by ANNOtate VARIation annotation. Mouse genome reads were filtered, as well as single-nucleotide polymorphisms (using dbSNP and 1000 genome data sets). All detected variants were manually checked.

Exome-Seq

DNA was isolated from fresh cell pellets washed in 1x PBS, using the QIAmp DNA Mini kit (Qiagen, Hilden, Germany) according to the manufacturer's protocol. DNA libraries were prepared using the Agilent (Santa Clara, CA, USA) SureSelect XT Library Prep Kit according to the manufacturer's protocol. Target enrichment was performed using the Agilent SureSelect XT Human All Exon v5 capture set. Sequencing with 100 base paired end reads of targeted enrichment libraries was performed on the HiSeq 2500 sequencer. A quality check of the raw data was performed by the FastQC tool (<http://www.bioinformatics.babraham.ac.uk/projects/fastqc/>). Reads were filtered first by quality using FASTX-Toolkit (v. 0.0.14, http://hannonlab.cshl.edu/fastx_toolkit/index.html) and then by length using HOMER (La Jolla, San Diego, CA, USA) (v. 4.7). The remaining reads were mapped to the Sanger human reference (hg19) by bwa (v. 0.6.2) with default settings. The resulting binary alignment map files were processed using SAMtools (San Francisco, CA, USA) (v. 0.1.19) and the Genome Analysis ToolKit (GATK) release 3.2.0. (Cambridge, MA, USA). In brief, binary alignment map files were binary compressed, sorted, and indexed by SAMtools (samtools view, sort, and index tools), duplicated reads were then removed by the SAMtools function rmdup, and base quality score recalibration and local realignment around indels followed the recommended workflow of the GATK toolkit (RealignerTargetCreator, IndelRealigner, BaseRecalibrator and PrintReads). Variants were called by VarScan (v2.3.7) with the following parameters: minimum variant allele frequency of 5%, a minimum coverage of 10 reads, at least 7 reads that confirm the mutation and a *P*-value below 0.05. Annotation of the vcf files was performed with ANNOtate VARIation. Variants were filtered: variant positions must not be listed as a single-nucleotide polymorphism in the 1000 genome project; variant position must be annotated as exonic by RefSeq (Release 45); and synonymous/nonsynonymous calls were made and the synonymous excluded from further analysis. All filtering was performed using in house parsers.

Digital droplet PCR

To determine the frequency of the mutation E193Q in LRRC69, L11V in CCDC151 and P934L in FLT3, DNA samples were analyzed by the ddPCR system QX100 from Bio-Rad (Hercules, CA, USA) according to and with reagents from the manufacturer.

The DNA oligos used were designed and supplied by Applied Biosystem (Foster City, CA, USA) (custom TaqMan single-nucleotide polymorphism genotyping assays). Amplification oligos for LRRC69 E193Q were 5'-GAAGCTTTTGTAGCCAGAAACAA-3' and 5'-AGCAAACACTGTGGTTCCATGTT-3', whereas wild-type and mutant-specific probes were 5'-TTTGGCCGAGGTAAG-3' (-VIC) and 5'-TTGCCGAGGTAAG-3' (-FAM), respectively. For CCDC151 L11V, amplification oligos were 5'-TCCACACCACACATGCA-3' and 5'-GGCCTCGTGTAGGTGTGAAC-3', whereas wild-

type and mutant-specific probes were 5'-CACCTCAGTTTCTTAC-3' (-VIC) and 5'-CACCTCACTTCTTAC-3' (-FAM), respectively. For FLT3 P934L, amplification oligos were 5'-GCTGGGCTTTTGAAGCAAGGA-3' and 5'-CATCTGCCAGCTGACATCCTAAAA-3', whereas wild-type and mutant-specific probes were 5'-TAGGGAAGGATGGCCGTT-3' (-VIC) and 5'-TAGGG AAGGATAGCCGTT-3' (-FAM), respectively. A gradient analysis revealed that the optimal annealing temperature for these oligo-sets was 59 °C for LRR69 E193Q and FLT3 P934L, and 60 °C for CCDC151 L11V. Genomic DNA samples were prepared with the QIAamp DNA Mini kit from Qiagen and digested with EcoNI (New England Biolabs, Ipswich, MA, USA) for LRR69 mutations and EcoRI (Sigma-Aldrich) for CCDC151 and FLT3 mutations. Duplicate reactions for analysis of samples prepared from *in vitro* grown clones contained 250 ng of DNA each. The analysis of PC-PDX21 and PC-PDX27 DNA were performed on pooled data from 15 reactions for each condition with 500 ng DNA in each well.

The DNA probes for detecting the different KRAS mutations were supplied by Bio-Rad Laboratories (ddPCR probes for mutation detection in human). Droplets were thermal cycled according to the manufacturer's protocol. The references for the different probes were: WT: dHsaCP2500597; G12D: dHsaCP2500596; G12V: dHsaCP2500592; G12R: dHsaCP2500590.

CONFLICT OF INTEREST

The authors declare no conflict of interest.

ACKNOWLEDGEMENTS

We thank Faye Su from Novartis and Daniel Pierce from Celgene for providing reagents and valuable insights. This work was supported by funds from the Instituto de Salud Carlos III (PI16/00253 and CIBER-ONC). KP was supported by the postdoctoral program from the AECC. FB was supported by the AGAUR-FI DGR-2014 predoctoral fellowship.

REFERENCES

- 1 Ryan DP, Hong TS, Bardeesy N. Pancreatic adenocarcinoma. *N Engl J Med* 2014; **371**: 1039–1049.
- 2 Burris HA, Moore MJ, Andersen J, Green MR, Rothenberg ML, Modiano MR *et al*. Improvements in survival and clinical benefit with gemcitabine as first-line therapy for patients with advanced pancreas cancer: a randomized trial. *J Clin Oncol* 1997; **15**: 2403–2413.
- 3 Hoff, Von DD, Ervin T, Arena FP, Chiorean EG, Infante J, Moore M *et al*. Increased survival in pancreatic cancer with nab-paclitaxel plus gemcitabine. *N Engl J Med* 2013; **369**: 1691–1703.

- 4 Biankin AV, Waddell N, Kassahn KS, Gingras M-C, Muthuswamy LB, Johns AL *et al*. Pancreatic cancer genomes reveal aberrations in axon guidance pathway genes. *Nature* 2012; **491**: 399–405.
- 5 Collins MA, Bednar F, Zhang Y, Brisset J-C, Galbán S, Galbán CJ *et al*. Oncogenic Kras is required for both the initiation and maintenance of pancreatic cancer in mice. *J Clin Invest* 2012; **122**: 639–653.
- 6 Xue W, Zender L, Miething C, Dickins RA, Hernando E, Krizhanovsky V *et al*. Senescence and tumour clearance is triggered by p53 restoration in murine liver carcinomas. *Nature* 2007; **445**: 656–660.
- 7 Collisson EA, Trejo CL, Silva JM, Gu S, Korkola JE, Heiser LM *et al*. A central role for RAF->MEK->ERK signaling in the genesis of pancreatic ductal adenocarcinoma. *Cancer Discov* 2012; **2**: 685–693.
- 8 Weisenberger DJ. Characterizing DNA methylation alterations from the Cancer Genome Atlas. *J Clin Invest* 2014; **124**: 17–23.
- 9 Missiaglia E, Donadelli M, Palmieri M, Crnogorac-Jurcevic T, Scarpa A, Lemoine NR. Growth delay of human pancreatic cancer cells by methylase inhibitor 5-aza-2'-deoxycytidine treatment is associated with activation of the interferon signalling pathway. *Oncogene* 2005; **24**: 199–211.
- 10 Kopetz S, Kopetz S, Lemos R, Lemos R, Powis G, Powis G. The promise of patient-derived xenografts: the best laid plans of mice and men. *Clin Cancer Res* 2012; **18**: 5160–5162.
- 11 Kim MP, Evans DB, Wang H, Abbruzzese JL, Fleming JB, Gallick GE. Generation of orthotopic and heterotopic human pancreatic cancer xenografts in immunodeficient mice. *Nat Protoc* 2009; **4**: 1670–1680.
- 12 Fisher R, Pusztai L, Swanton C. Cancer heterogeneity: implications for targeted therapeutics. *Br J Cancer* 2013; **108**: 479–485.
- 13 Byrne AT, Alferez DG, Amant F, Annibaldi D, Arribas J, Biankin AV *et al*. Interrogating open issues in cancer precision medicine with patient-derived xenografts. *Nat Rev Cancer* 2017; **17**: 254–268.
- 14 Olive KP, Jacobetz MA, Davidson CJ, Gopinathan A, McIntyre D, Honess D *et al*. Inhibition of Hedgehog signaling enhances delivery of chemotherapy in a mouse model of pancreatic cancer. *Science* 2009; **324**: 1457–1461.
- 15 Gore J, Korc M. Pancreatic cancer stroma: friend or foe? *Cancer Cell* 2014; **25**: 711–712.
- 16 Özdemir BC, Pentcheva-Hoang T, Carstens JL, Zheng X, Wu C-C, Simpson TR *et al*. Depletion of carcinoma-associated fibroblasts and fibrosis induces immunosuppression and accelerates pancreas cancer with reduced survival. *Cancer Cell* 2014; **25**: 719–734.
- 17 Rhim AD, Oberstein PE, Thomas DH, Mirek ET, Palermo CF, Sastra SA *et al*. Stromal elements Act to restrain, rather than support, pancreatic ductal adenocarcinoma. *Cancer Cell* 2014; **25**: 735–747.
- 18 Van Cutsem E, Hidalgo M, Bazin I, Canon J-L, Poddubskaya E, Manojlovic N *et al*. Phase II randomized trial of MEK inhibitor pimasertib or placebo combined with gemcitabine in the first-line treatment of metastatic pancreatic cancer. *J Clin Oncol* 2015; **33**; (Suppl3); Abstract 344.
- 19 Borroto A, Ruiz-Paz S, la Torre de TV, Borrell-Pages M, Merlos-Suarez A, Pandiella A *et al*. Impaired trafficking and activation of tumor necrosis factor- α -converting enzyme in cell mutants defective in protein ectodomain shedding. *J Biol Chem* 2003; **278**: 25933–25939.

Supplementary Information accompanies this paper on the Oncogene website (<http://www.nature.com/onc>)